Feature-independent Encoding of Visual Salience in the Mouse Superior Colliculus

Ruixiang Wu[1], Jinhuai Xu[1], Chunpeng Li[1,2], Zhaoji Zhang[1,3], Ling-yun Li[1,4], Ya-tang Li[1*]
[1]Chinese Institute for Brain Research, Beijing 102206, China
[2]College of Biological Sciences, China Agricultural University, Beijing 100193 China
[3]College of Chemistry and Molecular Engineering, Peking University, Beijing 100091, China
[4]Department of Neurobiology, School of Basic Medical Sciences,
Capital Medical University, Beijing 100069, China
*Correspondence: yatangli@cibr.ac.cn

Abstract

Detecting conspicuous stimuli in a visual scene is crucial for animal survival, yet it remains debated how the brain encodes visual salience. Here we investigate how visual salience is represented in the superficial superior collicular (sSC) of awake mice using two-photon calcium imaging. We report on a feature-independent salience map in the sSC. Specifically, conspicuous stimuli evoke stronger responses in both excitatory and inhibitory neurons compared to uniform stimuli, with similar encoding patterns observed in both neuron types. The largest response occurs when a salient stimulus is positioned at the receptive field center, with contextual effects extending $\sim$40° away from the center. The response amplitude correlates well with the salience strength of stimuli and is not influenced by the orientation or motion direction preferences of neurons. Furthermore, visual salience is encoded in a feature-independent manner, and neurons involved in salience encoding are less likely to exhibit orientation or direction selectivity.

Keywords: superior colliculus, visual salience, two-photon calcium imaging, feature-independent encoding

1 Introduction

Humans extract $\sim$20 bits of information from one gigabit of visual data that enter the eyes to guide behavior [1]. This sifting processing relies on visual attention and is essential for animals to survive in a complex and ever-changing environment. Visual attention has two types: endogenous (goal-driven/top-down) attention and exogenous (scene-driven/bottom-up) attention. Exogenous attention is naturally directed towards salient objects that "pop out" in the scene [2, 3, 4, 5, 6].

Salience, defined as the conspicuousness of a specific visual area within a scene, can arise from various physical attributes, such as orientation, color, motion direction, size, and shape. It is still under debate where and how visual salience is encoded in the brain. According to a theoretical model, the brain has a salience map that integrates inputs from diverse feature maps and represents salience strength in a manner independent of specific features [7, 8]. This salience map merges with goal-driven attention to generate a priority map reflecting the attended location [9, 10]. In primates, multiple brain regions have been identified as encoding visual salience, including the primary visual cortex (V1) [11, 12, 13, 14], the superficial and intermediate layers of superior colliculus (sSC and iSC) [15], V4 [16], the posterior parietal cortex [17], and the frontal eye field [18]. However, except for the sSC and V1, these regions also encode endogenous attention, suggesting that they might inherit the saliency map from upstream brain regions and host a priority map [19].

Preprint. Under review.

While the model predicts that the response of an ideal salience-encoding neuron is independent of specific visual features, there is a lack of direct experimental evidence from both V1 and sSC. In the V1 of both anesthetized and awake cats and monkeys, salient stimuli made by orientation have elicited larger, similar, or smaller responses compared to iso-orientation stimuli [12, 13, 20, 21, 22]. Similar inconsistencies have been observed in responses to salient stimuli made by motion direction[14, 23, 24]. However, these contradictions can be resolved if one takes the feature preference into account, suggesting that V1 neurons encode visual silence in a feature-dependent manner. In the sSC of awake monkeys, neural activity in response to salient stimuli correlates with salience strength, but the influence of feature preference remains unclear [15]. In the mouse sSC, neuronal responses also encode visual salience; however, encoding is affected by anesthesia [25, 26]. Additional factors that could affect the conclusion include whether the cortex is intact and the number of neurons recorded.

In the present work, we carried out *in vivo* two-photon calcium imaging in the sSC of head-fixed awake mice with an intact cortex. Our aim was to understand how the encoding of visual salience is contributed by excitatory and inhibitory neurons across different depths. Specifically, we aimed to elucidate how salience encoding is affected by different visual features by presenting salient stimuli based on either orientation or motion direction. Calcium responses of different cell types were assessed by expressing non-floxed GCaMP8 in the mouse sSC with genetically labeled GABAergic or glutamatergic neurons. Our findings demonstrate feature-independent encoding of visual salience by excitatory and inhibitory neurons across the depth of the mouse sSC.

2 Results

2.1 Excitatory and inhibitory neurons respond strongly to salient stimuli

To investigate how visual salience is encoded in the mouse sSC, we applied two-photon calcium imaging to measure the responses of both excitatory and inhibitory neurons to salient stimuli in head-fixed awake mice (Fig. 1a-c) [27]. We imaged the posterior-medial SC while leaving the cortex intact as previously described [28, 29]. Across 54 image planes and up to a depth of 300 μm, we recorded a total of 2565 excitatory neurons and 4455 inhibitory neurons in seven animals. Throughout the imaging session, the animal exhibited occasional locomotion and eye movements (Fig. 6a and d). During periods of locomotion, we observed a positive correlation between pupil size and locomotion speed, and neuronal responses showed either a negative or positive correlation with pupil size (Fig. 6b and c), consistent with previous findings [30].

Excitatory and inhibitory neurons were distinguished by expressing tdTomato in either Vglut2+ or Vgat+ neurons (Fig. 1d). In both lines, the percentage of excitatory neurons was 40%, in line with fluorescence *in situ* hybridization data [31]. To examine how neurons encode visual salience, we measured their calcium responses to a salient flashed grating (SFG) at the RF center against a vertical or horizontal background. Both excitatory and inhibitory neurons show stronger responses to the salient stimulus compared to the background alone (Fig. 1e), indicating a significant role of the sSC in encoding visual salience.

2.2 Neural encoding of visual salience is independent of orientation preference

Given the retinotopic organization and orientation preference of neurons in sSC, a neuron's response to an SFG is determined by three factors: 1) the distance between its RF center and the SFG; 2) the orientation contrast between the SFG and the background; 3) its orientation preference. To explore the impact of these factors on neuronal responses, we measured the RF and orientation preference of each neuron, along with their responses to an SFG at different spatial locations. Notably, the SFG at the RF center elicits the largest responses for both excitatory and inhibitory neurons, with the response amplitude gradually decreasing as its distance from the RF center increased (Fig. 2a, 2b, 7c). This suggests that these neurons function as detectors of visual salience rather than as edge detectors.

To disentangle the contributions of orientation contrast and preference, we sorted neuronal responses according to their preference for vertical or horizontal orientation. Intriguingly, for both excitatory and inhibitory neurons, the response amplitude at the RF center remains constant regardless of whether the background orientation is preferred or orthogonal (Fig. 2c, 2d, 7d), indicating that salience encoding in the sSC is independent of orientation preference. As the target moves away from the RF center, the response amplitude progressively decreases, up to $\sim$40°. For the preferred

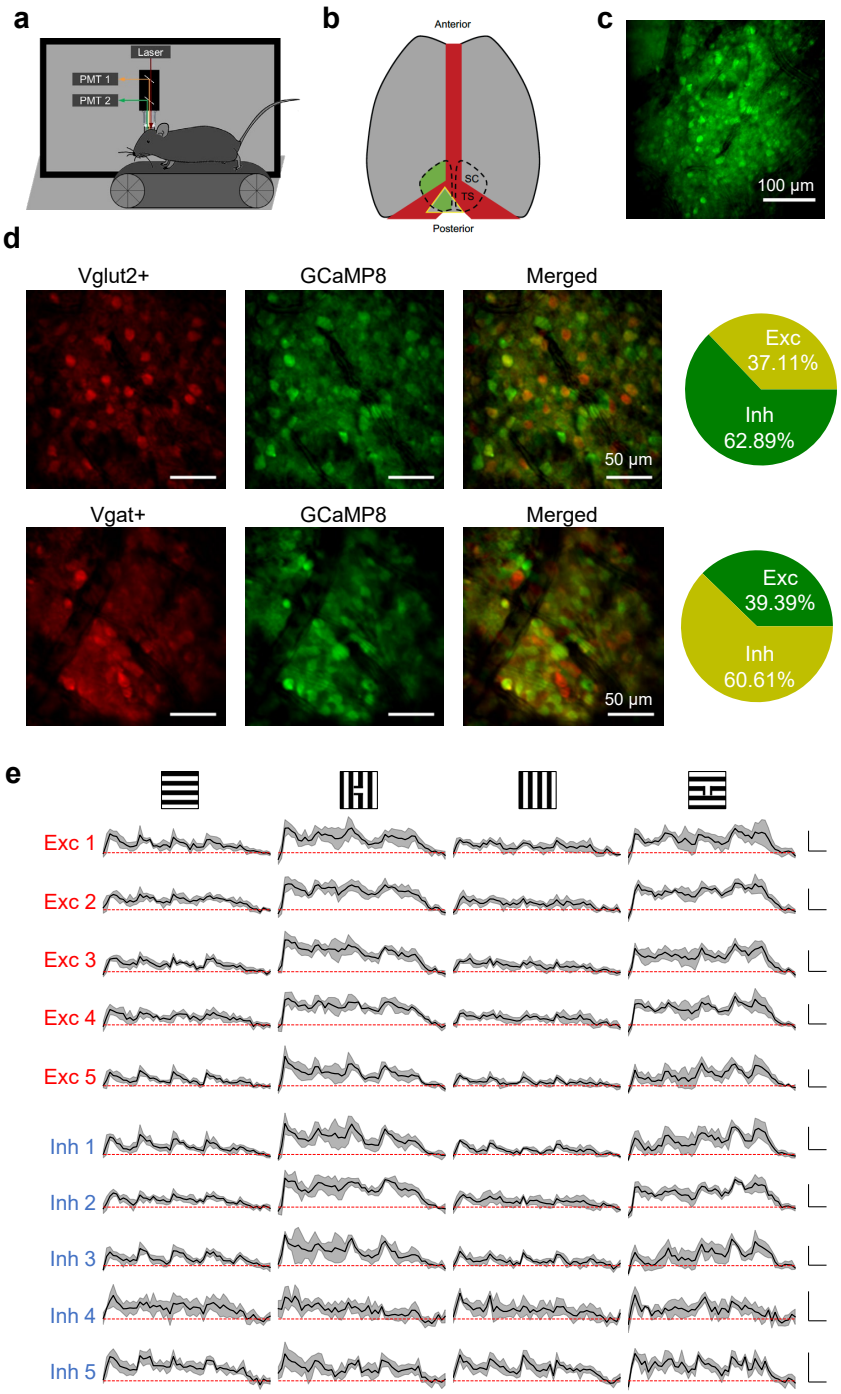

Figure 1: **Two-photon calcium imaging reveals robust visual responses to salient stimuli in the awake mouse superior colliculus. a.** Schematic of the experimental setup. Mice were head-fixed and free to run on a treadmill. Visual stimuli were presented on a screen. Neuronal calcium activity was imaged using two-photon microscopy. PMT, photomultiplier tube. **b.** Schematic of mouse brain anatomy after insertion of a triangular transparent plug to expose the posterior-middle portion of the superior colliculus beneath the posterior cortex. TS: transverse sinus. **c.** A standard deviation projection of calcium responses to visual stimuli in one field of view. **d.** A mean projection of tdTomato-labeled Vglut2+ or Vgat+ neurons and GCaMP8+ neurons in two mice. The right panel shows the proportion of excitatory and inhibitory neurons in both Vglut2-tdTomato and Vgat-tdTomato mice. **e.** Response profiles of 5 excitatory neurons and 5 inhibitory neurons to flashing gratings with and without a salient stimulus. Scale: 30% $\Delta F/F_0$, 1 s.

orientation, the response amplitude becomes comparable to that evoked by the background when the distance reaches $\sim$10°, the typical RF size of sSC neurons [32, 33]. A further decline in amplitude indicates a long-range suppression effect from the target to a visual location that is up to $\sim$40° away. Conversely, a long-range facilitation effect was observed for the orthogonal orientation, as evidenced by a larger response amplitude at a distance of $\sim$40° compared to that evoked by the orthogonal background. This contrasting long-range effect for preferred and orthogonal orientations may be implemented by local inhibitory neurons and wide-field excitatory neurons with dendrites extending up to $\sim$500 μm [34].

To assess the proportion of neurons involved in salience encoding, we calculated the salience index (SI) for each neuron (see Methods) and revealed that $\sim$80% of both excitatory and inhibitory neurons had an SI>0 (Fig. 2e). When considering only these neurons, the relationship between response amplitude and distance to the RF center mirrors that observed for all neurons (Fig. 7c). At last, salience encoding remains consistent across different depths within the sSC (Fig. 7e and f).

2.3 Neuronal responses are modulated by the salience strength

An ideal salience-encoding neuron should not only show a robust response to a conspicuous stimulus but also have its response amplitude correlate with the salience strength of the stimulus. To examine whether neurons in sSC meet this criterion, we systematically changed the orientation of the target against a fixed vertical or horizontal background, with an orientation contrast of 90° indicating the maximal salience strength. Our findings indicated that neuronal responses indeed reflect the orientation contrast rather than the absolute orientation of the target at the RF center (Fig. 3a and d). To quantify the contributions of orientation contrast, we aligned neuronal responses to their preferred orientations for both excitatory and inhibitory neurons. One can find that the response amplitude gradually decreases when the orientation contrast deviates from 90°, with the orientation preference exerting subtle or no influence on the amplitude (Fig. 3b and e). Note that the response amplitude evoked by the SFG with a 30° contrast is either smaller (for excitatory neurons) or comparable (for inhibitory neurons) when compared to the response evoked by the preferred background. This finding aligns with the notion that the salience encoding is independent of feature preference (Fig. 2) and corresponds to findings observed in the V1 of cats and monkeys [14]. This independence is reinforced by averaged SFG-evoked responses aligned to the preferred orientation of each neuron (Fig. 3c and f).

2.4 Salience encoding is independent of specific visual features

Salience in visual stimuli can be induced by different features, such as orientation, motion direction, and color. To explore whether the orientation preference-independent encoding of salience extends to other features, we measured and analyzed neuronal responses to a salient moving grating (SMG). Similar to SFG-evoked responses, neurons exhibit the strongest responses when the target is at the RF center (Fig. 4a and b), and the response amplitude to an SMG does not depend on their preference of motion direction (Fig. 4c and d). To probe how different visual features contribute to salience encoding, we compared neuronal responses evoked by an SMG with those evoked by an SFG. The strong correlation between them indicates that the same group of neurons encode both orientation-induced and direction-induced salience (Fig. 4e). In other words, neural encoding of visual salience is independent of specific visual features. It is worth noting that the relative response amplitude to an SMG is larger than that to an SFG (Fig. 4e), and there are $\sim$65% of neurons that have SI>0 (Fig. 4f). These differences may be attributed to the challenges inherent in quantifying the strength of visual salience made by different features.

2.5 Salience-encoding neurons are not feature-selective

Neurons tuned to specific visual features, such as orientation and motion direction, form a functional map in the mouse SC [28, 35, 36, 29]. How does this feature encoding relate with salience encoding? For the same group of neurons, we plotted their orientation map, direction map, and salience maps (Fig. 5a). In the salience map, the salience strength at different locations is indicated by SI. We found that neurons showing strong orientation or direction selectivity are more likely to have negative SI and show weak responses to salient stimuli (Fig. 5a and 8a). Indeed, both OSI and DSI are negatively correlated with SI for both excitatory and inhibitory neurons (Fig. 5b and c), indicating that visual

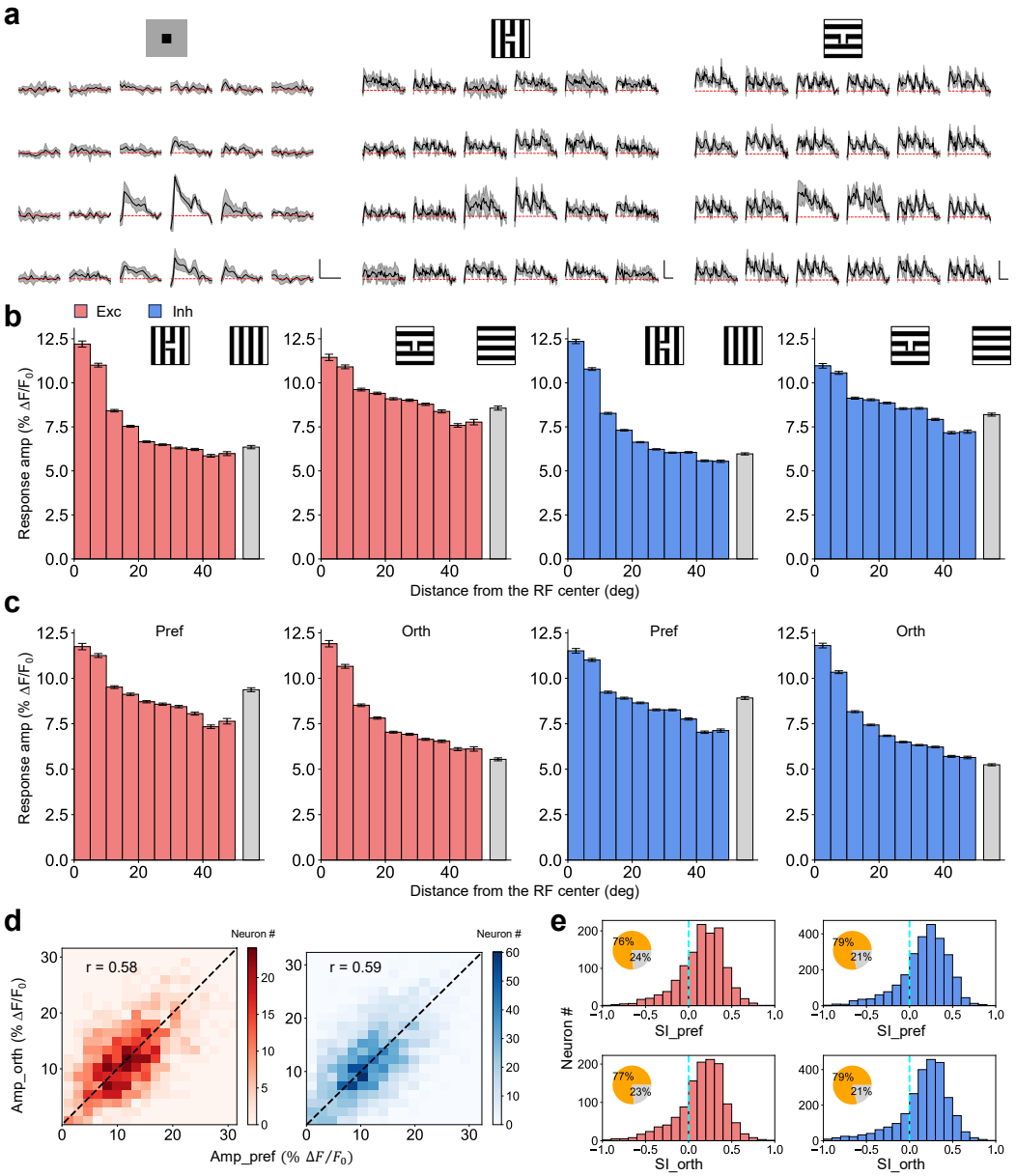

Figure 2: **Salience encoding is independent of orientation preference. a.** Calcium responses of an example neuron to flashed squares, flashed horizontal and vertical gratings against an orthogonal background. Scale: 30% Δ F/F$_0$, 1 s. **b.** Response amplitude to SFGs with the target at different distances from the RF center (colored bars), as well as the amplitude to the background (gray bars) for both excitatory and inhibitory neurons. **c.** Response amplitude to SFGs and the background sorted by orientation preference. **d.** Response amplitude at the orthogonal orientation versus that at the preferred orientation (Exc: r= 11.9 ± 5.5 vs. 11.8 ± 5.6; Inh: 11.7 ± 6.0 vs. 11.6 ± 5.9). The black lines indicate the identity line, while the cyan lines indicate the linear fitting. Their relationship is quantified by Pearson's correlation coefficient (r) with p<0.001 for both correlations. **e.** The proportion of neurons with SI>0 at both preferred and orthogonal orientations for both types.

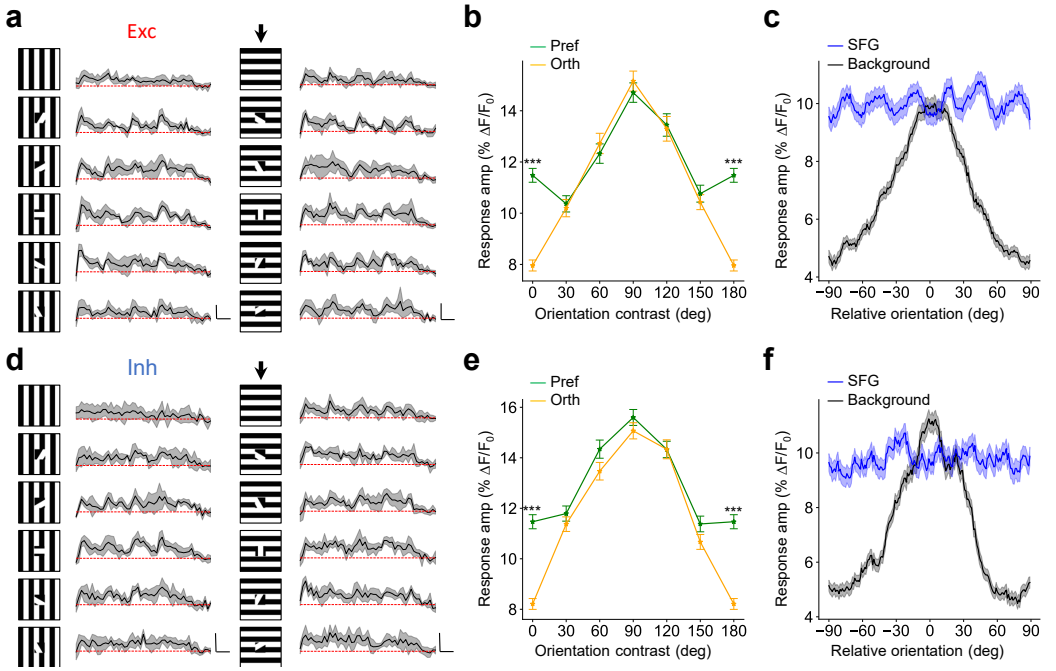

Figure 3: **Neurons in the sSC encode salience strength. a.** Response profiles of an example excitatory neuron to SFGs with 6 different orientation contrasts in two backgrounds. **b.** Averaged calcium responses to different orientation contrasts in preferred and orthogonal backgrounds for neurons with SI>0. Error bars represent SEM. *** indicates p<0.001, paired t-test, N=136. **c.** The averaged responses evoked by the SFG and the background aligned to the preferred orientation of each neuron. **d-f.** The same plots as **a-c** for inhibitory neurons, N=169.

features and salience are encoded by largely distinct neural ensembles. This anticorrelation can not be attributed to the amplitude at the preferred orientation or direction. First, both OSI and DSI are negatively correlated with the response amplitude evoked by SFG or SMG (Fig.8a-c). Second, feature selectivity is mainly contributed by a decrease at the orthogonal orientation or null direction (Fig.8d and e).

3 Discussion

Cracking the neural encoding of visual salience is important for understanding how useful information is extracted from massive visual input, and such an extracting process is crucial for animals to survive and thrive in an ever-changing environment. In this study, we investigate how excitatory and inhibitory neurons in sSC encode visual salience made by different visual features.

3.1 Main findings

To uncover how visual salience is encoded in the sSC, we applied two-photon calcium imaging to measure the responses of both excitatory and inhibitory neurons in awake mice to salient visual stimuli. We found that excitatory and inhibitory neurons show similar response properties in the awake state (Fig. 1). Specifically, a salient stimulus at the RF center of neurons evokes the strongest response amplitude, which progressively decreases as the stimulus moves away from the RF until the distance reaches $\sim$40° (Fig. 2). In addition, the response amplitude to salient stimuli made by orientation is unaffected by the orientation preference but is instead determined by the salience strength of the stimuli (Fig. 2 and 3). Furthermore, this preference-independent salience encoding extends to salient stimuli made by motion direction, and the response amplitude evoked by these two types of stimuli is highly correlated (Fig. 4). These results indicate that the salience encoding in the sSC is not only independent of neurons' orientation and direction preferences but also independent of different features that induce visual salience, as predicted by the theory [7]. Further analysis suggests

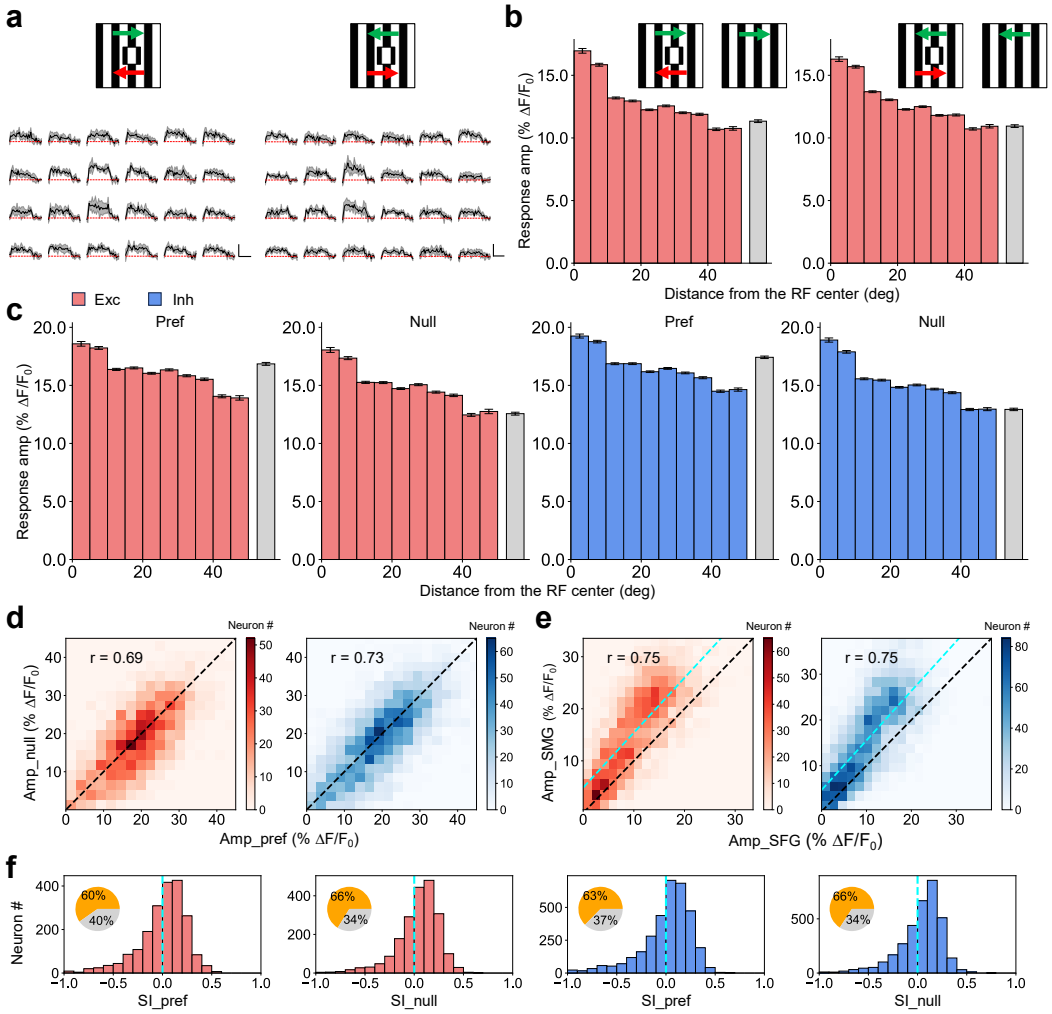

Figure 4: **Encoding of visual salience is independent of motion direction preference and specific visual features. a.** Calcium responses of an example neuron to moving gratings against a background moving in the opposite direction. Green arrows indicate the motion direction of the background, and red arrows indicate the direction of the target. Scale: 30% Δ F/F$_0$, 1 s. **b.** Response amplitude to SMGs with the target at different distances from the RF center (red bars) and the amplitude to the background (gray bars) for excitatory neurons. **c.** Response amplitude to SMGs and the background sorted by motion direction preference. **d.** Responses amplitude at the null direction versus that at the preferred direction (Exc: 18.3 ± 8.6 vs. 18.8 ± 8.0; Inh: 18.9 ± 9.2 vs. 19.4 ± 9.0). Black lines are the identity line, and cyan lines indicate the linear fitting. The Pearson's correlation coefficient (r) is significant (p<0.001) for both correlations. **e.** Response amplitude to SMGs versus that to SFGs, and with a significant correlation for both types (p<0.001). **f.** The proportion of neurons with SI>0 at both the preferred and null directions for both excitatory and inhibitory neurons.

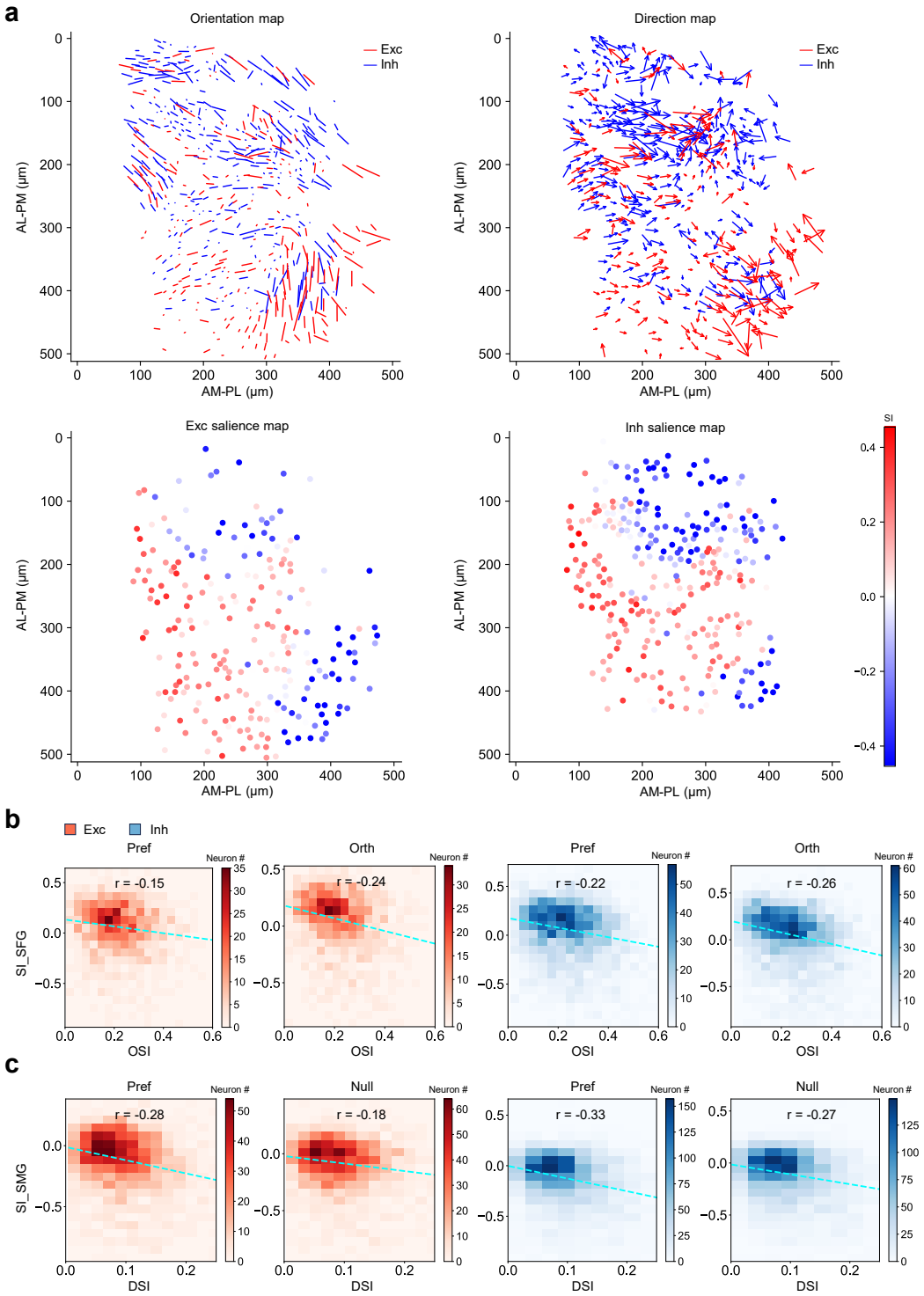

Figure 5: **Neurons that encode salience are less selective to orientation and motion direction** **a.** Upper panels show the orientation map and direction map represented by excitatory (red) and inhibitory (blue) neurons in an imaging plane. The length of the lines or arrows proportionally correlates with OSI or DSI. Lower panels show the salience map represented by excitatory and inhibitory neurons in the same plane. **b.** SI is anti-correlated with OSI measured by flashing gratings: r is Pearson's correlation coefficient, p<0.001 for all correlations. **c.** SI is anti-correlated with DSI measured by moving gratings: p<0.001 for all correlations.

that salience-encoding neurons and feature-encoding neurons belong to distinct neural ensembles (Fig. 5).

3.2 Relation to prior work

Prior work indicates that salience encoding in V1 is dependent on specific visual features [12, 13, 21, 14, 37]. Neurons in cat and monkey V1 are sharply tuned to visual features, such as orientation or motion direction [38, 39]. Their responses to salient stimuli are determined by both the strength of salience and their preference of orientation or motion direction [12, 13, 21, 14]. In contrast, neurons in the primate sSC are less tuned to visual features but show robust responses to salient locations in natural scenes [40, 41, 15], suggesting a feature-independent encoding of salience. Similarly, in rat sSC, the encoding of visual salience is not influenced by orientation preference [42]. In the optic tectum, the non-mammalian homologue of SC, neurons encode visual salience based on motion direction in a preference-independent manner but do not encode orientation-induced salience [43, 44, 45]. Here, we present direct evidence in mice supporting the notion that salience encoding in the sSC is not only independent of orientation or direction preference but also independent of specific visual features. Furthermore, salience-encoding neurons in mouse sSC are less feature-selective (Fig. 5), echoing similar findings in the primate sSC.

Note that the salience encoding in the sSC is affected by both anesthesia and cortical inputs [26]. In anesthetized mice, excitatory and inhibitory neurons in the sSC show opposite responses to motion contrast, with both types being suppressed by the orientation contrast [25]. However, in the awake state, our study demonstrates that excitatory and inhibitory neurons show similar responses to salient stimuli, consistent with recent findings showing strong responses to the edge of drifting or flashing gratings in both neuron types [46].

Moreover, the salience encoding is also influenced by the target size. In our study, the maximal response of sSC neurons is elicited by a salient stimulus of 10° at the RF center, indicating their role as salience detectors. However, when the target size exceeds the RF size, iso-feature suppression at the center causes the maximal response to be elicited by the edge, leading to neurons behaving as edge detectors [46].

3.3 Neural implementation of visual salience

In primate V1, visual salience is encoded in a feature-dependent manner. For a cortical neuron, when the orientation surrounding its RF matches its preferred orientation, iso-orientation stimuli within its RF elicit stronger responses than cross-orientation stimuli. Conversely, when the surrounding orientation is orthogonal to its preferred orientation, cross-orientation stimuli are more effective [12]. One can understand such contextual effects by convolving the visual stimulus with its subthreshold RF (Fig. 9), which reflects the integrated synaptic inputs and is larger than the spike RF [47].

However, the convolution fails to predict the feature-independent encoding of visual salience in the mouse sSC, which might be addressed by integrating long-range inhibition as proposed by the model. This long-range inhibition could be contributed by local inhibitory neurons with horizontally extended dendritic arbors reaching up to 500 μm, accounting for $\sim$60% of all neurons in the sSC [34, 31]. In contrast, inhibitory neurons in V1 exhibit heterogeneous morphologies and represent only $\sim$25% of the total neuronal population [48]. Another contributing factor could be functional patches in the sSC [28, 29]: first, the size of these patches is comparable to the observed long-range effect over $\sim$40° (Fig. 2a and 4c); second, the connection strength between neurons is affected by both their distance and functional similarity [49, 50, 51]. Additionally, wide-field excitatory neurons with large dendrites may also play a role in salience encoding [34]. Future modeling work may examine how these factors collectively contribute to the feature-independent salience map in the sSC.

The neural encoding of visual salience in the sSC could be contributed by direct inputs from the retina and V1. In the retina, salient stimuli made by orientation or motion direction elicit stronger responses in retinal ganglion cells (RGCs) compared to uniform stimuli [52, 53]. Importantly, the robust response of object motion sensitive (OMS) RGCs to salient moving stimuli is independent of direction preference [54, 55], indicating that salience encoding in sSC could be partially inherited from the retina, if not entirely. In contrast, cortical inputs from V1 reduce the distinction between responses evoked by cross-orientation and iso-orientation stimuli, thereby compromising the encoding capacity [26]. This implies that salience encoding in the sSC is less likely to rely on inputs from V1.

3.4 The role of superior colliculus in visual attention

In primates, the sSC plays a critical role in bottom-up attention and is not involved in arousal-related top-down attention [15, 19]. Supporting this notion, our data demonstrated that salience encoding is not affected by pupil size (Fig. 6e), a common indicator of an animal's arousal state [56]. The sSC projects to many brain regions, including the pulvinar, the lateral geniculate nucleus, and the intermediate layer of SC (iSC) [34, 57]. Additionally, iSC also receives inputs from the prefrontal cortex carrying top-down information [58], and neurons in iSC respond to stimuli from different sensory modalities [59]. Thus, iSC may serve as an ideal hub to integrate the feature-independent salience map from sSC with goal-driven attention to generate a modality-independent priority map that determines the attended location. Indeed, inactivating deep layers of the primate SC compromises the behavioral performance in visual-attention tasks [60]. One exciting research direction is to explore how the feature-independent visual salience map in sSC is transformed into the modality-independent priority map in iSC.

4 Materials and Methods

All experimental procedures were performed under the animal welfare guidelines and approved by the Institutional Animal Care and Use Committee at the Chinese Institute for Brain Research, Beijing.

4.1 Animal

Both male and female laboratory mice were used at ages 2-4 months. Vglut2-ires-Cre (JAX no. 028863) or Vgat-ires-Cre (JAX no. 028862) mice were crossed with an Ai14 mice (JAX no. 007914) line to express tdTomato in either excitatory (Vglut+) or inhibitory (Vgat+) neurons.

4.2 Viral injection

We injected adeno-associated virus (AAV) expressing non-floxed GCaMP8m (AAV2/9-syn-jGCaMP8m-WPR) into the SC of Vglut2-tdTomato and Vgat-tdTomato mice. After 2–3 weeks, we surgically implanted a cranial window coupled to a transparent silicone plug to expose the posterior-medial portion of the sSC, corresponding to the upper-temporal part of the visual field. After 3 days, we used two-photon microscopy to image calcium signals in the sSC of head-fixed awake mice.

4.3 *In vivo* two-photon calcium imaging

The animal was head-fixed on a treadmill and free to move. Following a 15-minute habituation period, two-photon imaging was performed using a microscope (Ultima 2P Plus, Bruker) with a $16\times$, 0.8 NA, 3 mm WD objective (CF175, Nikon). A tunable femtosecond laser (InSight X3+ Dual, Spectra-Physics) was raster scanned by resonant galvanometers. GCaMP8m and tdTomato were excited at 920 nm, with the laser power at the sample plane typically set between $30 - 50$ mW. A 550 μm $\times$ 550 μm field of view was scanned at 10 Hz as a series of 512 pixels $\times$ 512 pixels images, and the imaging depth was up to 350 μm. Emitted green and red light were split with a dichroic mirror (t565lpxr), passed through two bandpass filters (et525/70m-2p and et595/50m-2p), and detected by two GaAsP tubes (H10770PB-40, Hamamatsu). The animal's locomotion, pupil size, and positions were recorded and synchronized with the image acquisition. During the imaging session, the mice exhibited only rare eye movements and locomotion.

4.4 Visual stimulation

A 21-inch LED monitor was placed 17 cm away from the mouse's right eye, centered at 95° azimuth and 25° elevation, covering a visual field of 104° $\times$ 80°. To investigate how visual saliency is encoded in the sSC, we presented six types of visual stimuli in a 40° $\times$ 60° space that effectively covered the visual field recorded during each imaging session. **(1)** 4×6 (one at a time) 10° $\times$ 10° flashing squares (1 s black or white + 1 s grey) to map the receptive field (RF). **(2)** A full-field flashing square grating with a spatial frequency of 0.1 cycles per degree in 6 orientations and 4 phases (4 s grating + 1 s grey) to measure the orientation selectivity. **(3)** 4×6 (one at a time) 10° $\times$ 10° flashing square gratings in vertical (0°) or horizontal (180°) orientations on a grating background in the orthogonal orientation. **(4)** A 10° $\times$ 10° flashing square grating in 6 orientations at the RF center with a vertical or horizontal grating background. **(5)** A full-field moving square grating with a spatial frequency of 0.1 cycles per degree and a temporal frequency of 2 Hz in 12 directions measures the direction selectivity (2 s grating + 1 s grey). **(6)** 4×6 (one at a time) 10° $\times$ 10° moving gratings in 0°, 90°, 180°, and 270° directions on a grating background moving in the opposite directions. All stimuli were displayed for 10 repetitions, and the sequence was pseudo-randomized for each stimulus.

4.5 Data analysis

4.5.1 Measurement of calcium responses

Brain motion during imaging was corrected using NoRMCorre [61]. Regions of interest (ROIs) were manually drawn using the Cell Magic Wand Tool (ImageJ) and fitted with an ellipse in Python. Fluorescence traces of each ROI were extracted after estimating and removing contamination from surrounding neuropil signals as described previously [29, 62, 63]. The true fluorescence signal of a neuron was calculated as $F_{\text{true}} = F_{\text{raw}} - (r \cdot F_{\text{neuropil}})$, where r is the out-of-focus neuropil

contamination factor, estimated to be ~ 0.7 for our setup. Slow baseline fluctuations were removed using detrended fluctuation analysis with a 15-second sliding window.

For any given stimulus, the response of a neuron was defined by the fluorescence trace in its ROI during the stimulus period:

$$R = \frac{F - F_0}{F_0} \tag{1}$$

where F is the instantaneous fluorescence intensity and F_0 is the mean fluorescence intensity without visual stimulation (grey screen).

Two criteria were applied to interpret ROIs as neurons: 1) The size of the ROI was limited to 10-20 μm to match the size of a neuron; 2) The response from the ROI had to pass a signal-to-noise ratio (SNR) of 0.5 [33]:

$$SNR = \frac{\mathrm{Var}[\langle C \rangle_r]_t}{\langle \mathrm{Var}[C]_r \rangle_t} \tag{2}$$

where C is the N_t (time samples) $\times$ N_r (stimulus repetitions) response matrix, $t = 1, \ldots, N_t$ and $r = 1, \ldots, N_r$, $\langle \cdot \rangle_r$ and $\langle \cdot \rangle_t$ are the means over repetitions or time respectively, and $\mathrm{Var}[\cdot]_r$ and $\mathrm{Var}[\cdot]_t$ are the corresponding variances. All ROIs meeting these criteria were selected for further analysis, yielding a total of 7020 neurons, including 2565 excitatory neurons and 4455 inhibitory neurons.

4.5.2 Quantification of neuronal responses

To quantify the orientation tuning, we calculated the orientation selectivity index (OSI) as the normalized amplitude of the response-weighted vector sum of all orientations:

$$OSI = \frac{|\sum_k R(\theta_k) \times \mathrm{e}^{2i\theta_k}|}{\sum_k R(\theta_k)} \tag{3}$$

Where θ_k is the kth orientation in radians and $R(\theta_k)$ is the average response during the stimulus period at that orientation.

To quantify the tuning of a neuron to motion directions, we calculated the direction selectivity index (DSI) as the normalized amplitude of the response-weighted vector sum of all directions:

$$DSI = \frac{|\sum_k R(\rho_k) \times \mathrm{e}^{i\rho_k}|}{\sum_k R(\rho_k)} \tag{4}$$

Where ρ_k is the kth direction in radians and $R(\rho_k)$ is the average response during the stimulus period at that direction.

To quantify the preference for salient stimuli, we calculated the salience index (SI) as the relative difference between its response to SFG or SMG and that to the background in the preferred orientation or motion direction.

$$SI = \frac{R(s) - R(p)}{R(s) + R(p)} \tag{5}$$

Where $R(s)$ is the average response to a salient stimulus during the stimulus period, and $R(p)$ is the average response to the background of the preferred orientation or direction.

To quantify the RF size and locate its center, the calcium responses at 4×6 locations were fitted with a 2-D Gaussian function (Equation 6),

$$f = A \cdot \mathrm{e}^{-\frac{((x-E)\cos(D)-(y-F)\sin(D))^2}{2B^2} - \frac{((x-E)\sin(D)+(y-F)\cos(D))^2}{2C^2}} + G \tag{6}$$

The RF size is defined as the area at half of maximum, which equals $\pi \cdot 2 \ln 2 \cdot B \cdot C$. We omitted analysis of the RF if the coefficient of determination for this fit was below 0.5. We also the RF center as the center of mass for evoked responses and found consistent results with both approaches.

4.6 Neural modeling

For simplicity, the model was built in 1-D visual space with only two stimuli: positive and negative. Functional patches are simulated with a sinusoidal function, termed the feature selectivity index (FSI), which quantifies the preference of each neuron at different spatial locations. Since the OSI is mainly correlated with the response at the orthogonal orientation (Fig. 8d), we set a neuron's response amplitude to its preferred stimulus as 1, while its responses to non-preferred stimuli varied with FSI.

$$\mathbf{FSI} = \cos\left(\pi/\rho * \mathbf{v}\right) \tag{7}$$

Where ρ denotes the patch size set to 30°, and $\mathbf{v}$ is a vector representing the visual space of [-60°, 60°].

The RF of each neuron was simulated with a 1-D Gaussian function.

$$\mathbf{RF} = \exp(-\frac{(\mathbf{v} - \mu)^2}{2\sigma^2}) \tag{8}$$

Where μ is the location of the RF center in visual space, and σ is set to 5° for the subthreshold RF.

A neuron's response to a given visual stimulus is simulated by convolving its RF with the stimulus.

$$R = R_p \times (\mathbf{RF} \cdot \mathbf{vp}) + R_n \times (\mathbf{RF} \cdot \mathbf{vn}) \tag{9}$$

Where $\mathbf{vp}$ and $\mathbf{vn}$ are the positive and negative stimuli, and R_p and R_n are the response amplitude to the positive and negative stimuli.

5 Supplement

Here we report details related to the Results, Discussion, and Methods sections.

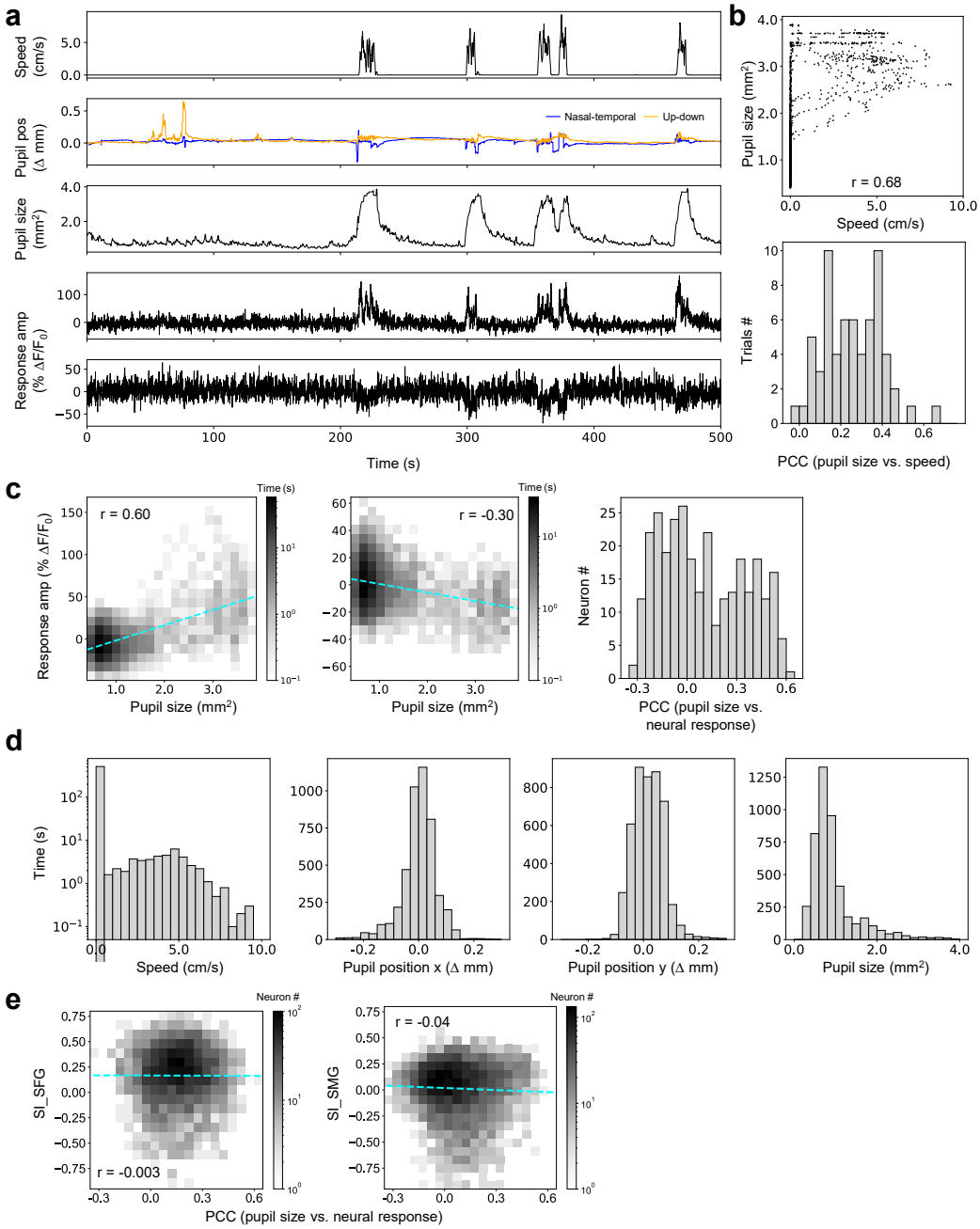

Figure 6: **Behavioral modulation of neuronal responses to salient stimuli (related to Fig. 1). a.** Locomotion speed, pupil positions, pupil size, and calcium responses in an example mouse. **b.** Top, Pupil size versus locomotion speed: r denotes the Pearson's correlation coefficient (PCC). Bottom, histogram of their PCC. **c.** Left, calcium responses of two example neurons versus pupil size. Cyan lines indicate the linear fitting. Right, histogram of their PCC. **d.** Histograms of locomotion speed, pupil positions, and pupil size for all animals. **e.** SI_SFG and SI_SMG versus PCC between pupil area and neural responses.

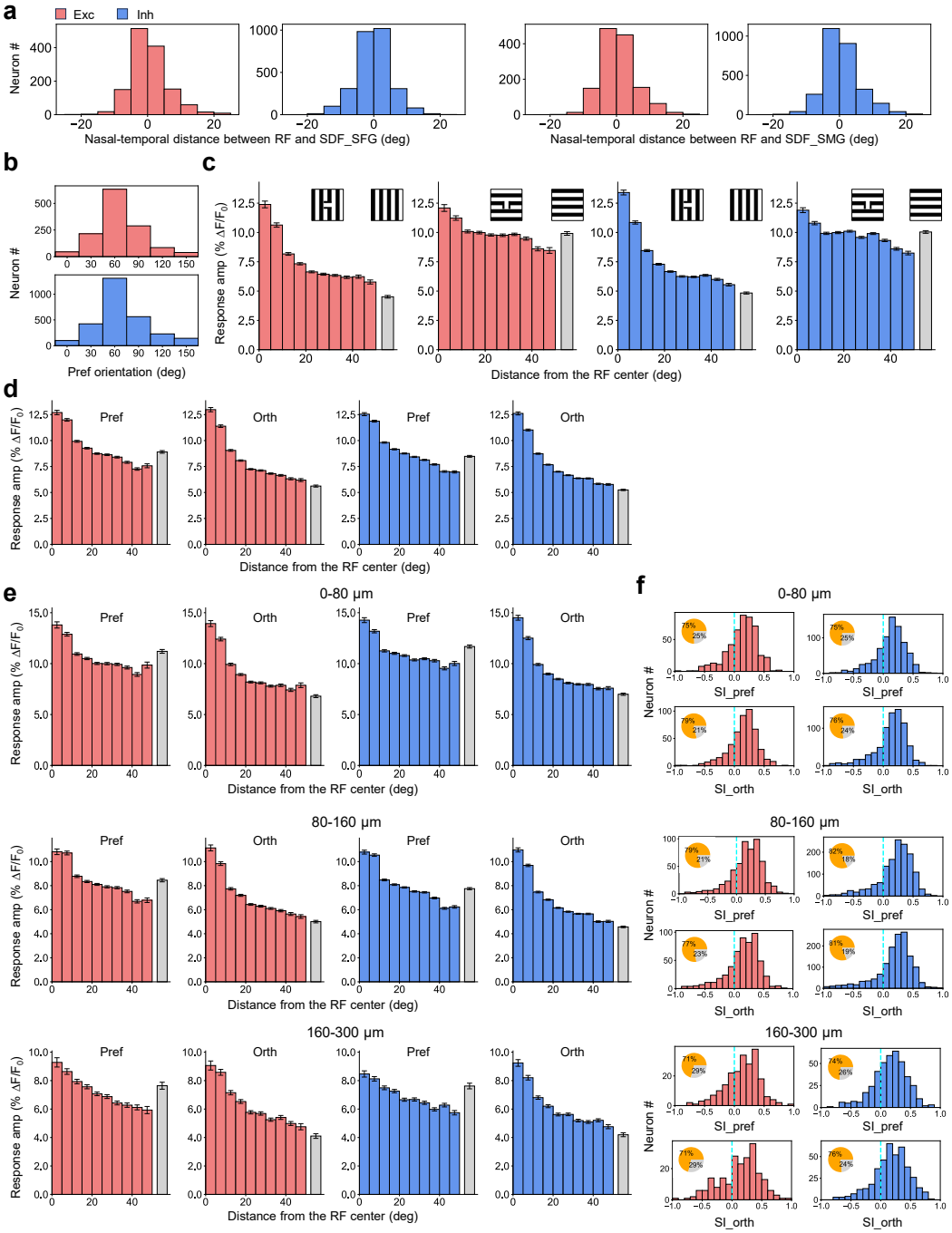

Figure 7: **Preference- and depth-independent salience encoding in the mouse sSC (related to Fig. 2). a.** The relative distance along the nasal-temporal axis between the RF center and the center of the salience detection field (SDF). The center of SDF is defined as the center of mass for SFG- or SMG-evoked responses (SDF_SFG or SDF_SMG). **b.** Histograms of the preferred orientation. **c.** The same plots as Fig. 2b for neurons with the preferred orientation of 90° ± 15°. Exc: N=448; Inh: N=896. **d.** The same plots as Fig. 2c for neurons with SI>0. Exc: N=929; Inh: N=1972. **e.** Response amplitude to SFG and the background grouped by orientation preference across the depth. **f.** Histograms of SI across the depth.

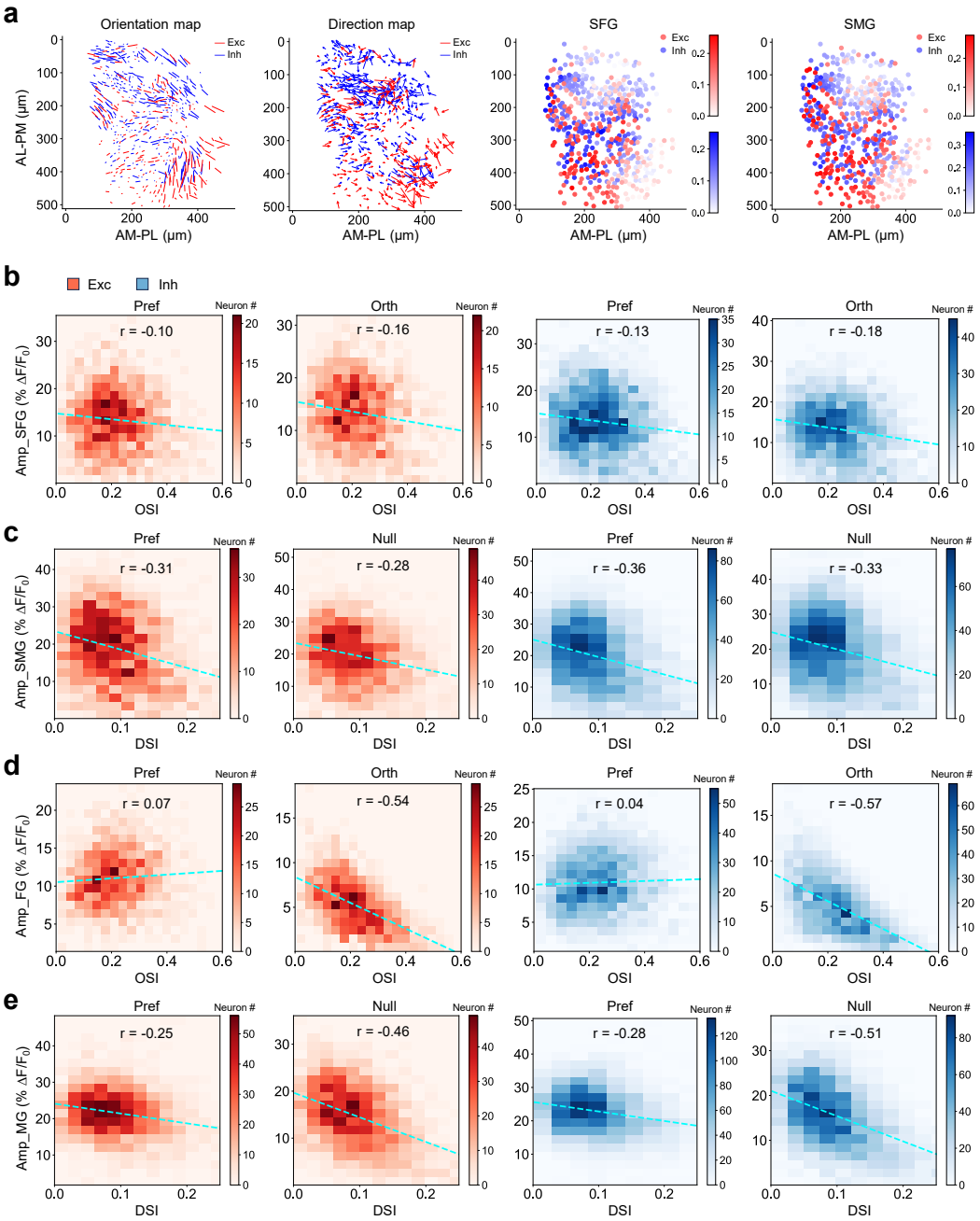

Figure 8: **Neurons tuned to the orientation and motion direction show weaker responses to salient stimuli compared to non-tuned neurons. a.** Left panels show the orientation map and direction map represented by excitatory (red) and inhibitory (blue) neurons in an imaging plane (the same as Fig.5a). The right part shows the response amplitude to SFG and SMG of the same group of neurons. **b.** Response amplitude to SFG is anti-correlated with OSI: r is Pearson's correlation coefficient, $p<0.001$ for all correlations. **c.** Response amplitude to SMG is anti-correlated with DSI: $p<0.001$ for all correlations. **d.** Response amplitude to flashed gratings (FG) at the preferred and orthogonal orientations versus OSI: $p<0.01$, <0.001, <0.05, <0.001 for correlations from left to right. **e.** Response amplitude to moving gratings (MG) at the preferred and null directions versus DSI: $p<0.001$ for all correlations.

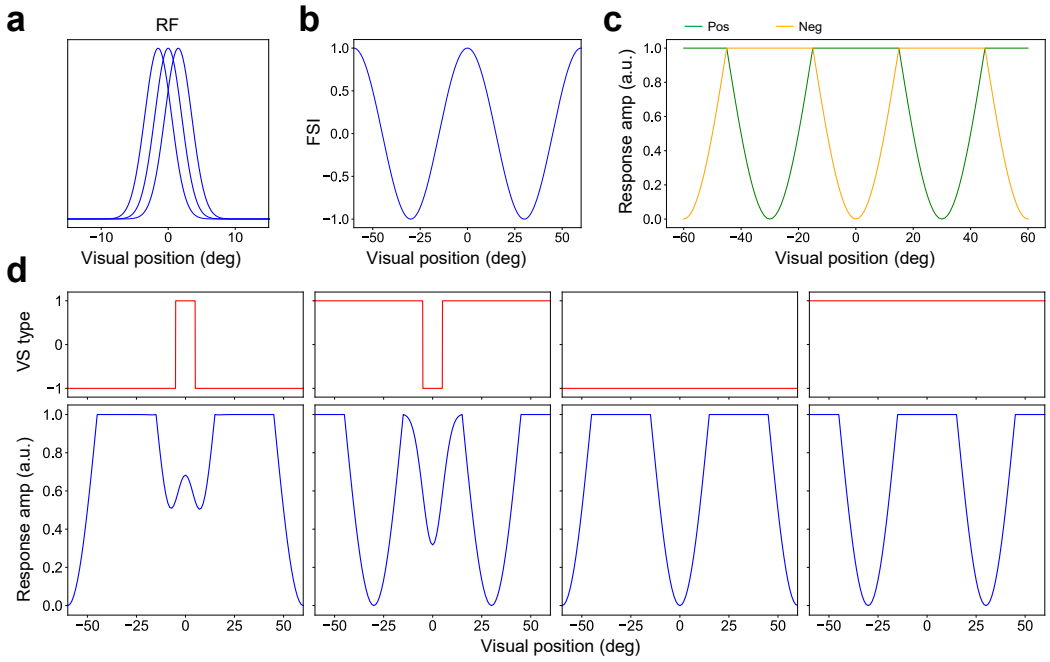

Figure 9: **Neural modeling for feature-dependent salience in V1. a.** Synaptic RFs for three nearby neurons. **b.** FSI of neurons in 1-D visual space. **c.** Neuronal responses to positive and negative stimuli. **d.** Top, four visual stimuli. Bottom, simulated neuronal responses in the visual space.

References

[1] Xaq Pitkow and Markus Meister. Neural Computation in Sensory Systems. In Michael S Gazzaniga and George R Mangun, editors, *The Cognitive Neurosciences*, pages 305–318. MIT Press, Cambridge, MA, 5th edition, 2014.

[2] Anne M. Treisman and Garry Gelade. A feature-integration theory of attention. *Cognitive Psychology*, 12(1):97–136, January 1980.

[3] Anne Treisman. Preattentive processing in vision. *Computer Vision, Graphics, and Image Processing*, 31(2):156–177, August 1985.

[4] Michael I. Posner. Orienting of attention. *The Quarterly Journal of Experimental Psychology*, 32(1):3–25, 1980. Place: United Kingdom Publisher: Taylor & Francis.

[5] Julian S. Joseph and Lance M. Optican. Involuntary attentional shifts due to orientation differences. *Perception & Psychophysics*, 58(5):651–665, July 1996.

[6] Derrick J. Parkhurst and Ernst Niebur. Texture contrast attracts overt visual attention in natural scenes. *European Journal of Neuroscience*, 19(3):783–789, 2004. _eprint: https://onlinelibrary.wiley.com/doi/pdf/10.1111/j.0953-816X.2003.03183.x.

[7] C. Koch and S. Ullman. Shifts in selective visual attention: towards the underlying neural circuitry. *Human Neurobiology*, 4(4):219–227, 1985.

[8] L. Itti, C. Koch, and E. Niebur. A model of saliency-based visual attention for rapid scene analysis. *IEEE Transactions on Pattern Analysis and Machine Intelligence*, 20(11):1254–1259, November 1998. Conference Name: IEEE Transactions on Pattern Analysis and Machine Intelligence.

[9] John T. Serences and Steven Yantis. Selective visual attention and perceptual coherence. *Trends in Cognitive Sciences*, 10(1):38–45, January 2006.

[10] Jillian H. Fecteau and Douglas P. Munoz. Salience, relevance, and firing: a priority map for target selection. *Trends in Cognitive Sciences*, 10(8):382–390, August 2006. Publisher: Elsevier.

[11] Xilin Zhang, Li Zhaoping, Tiangang Zhou, and Fang Fang. Neural Activities in V1 Create a Bottom-Up Saliency Map. *Neuron*, 73(1):183–192, January 2012.

[12] Yin Yan, Li Zhaoping, and Wu Li. Bottom-up saliency and top-down learning in the primary visual cortex of monkeys. *Proceedings of the National Academy of Sciences*, 115(41):10499–10504, October 2018. Publisher: National Academy of Sciences Section: Biological Sciences.

[13] J. J. Knierim and D. C. van Essen. Neuronal responses to static texture patterns in area V1 of the alert macaque monkey. *Journal of Neurophysiology*, 67(4):961–980, April 1992. Publisher: American Physiological Society.

[14] Adam M. Sillito, Kenneth L. Grieve, Helen E. Jones, Javier Cudeiro, and Justin Davls. Visual cortical mechanisms detecting focal orientation discontinuities. *Nature*, 378(6556):492–496, November 1995. Number: 6556 Publisher: Nature Publishing Group.

[15] Brian J. White, David J. Berg, Janis Y. Kan, Robert A. Marino, Laurent Itti, and Douglas P. Munoz. Superior colliculus neurons encode a visual saliency map during free viewing of natural dynamic video. *Nature Communications*, 8:14263, January 2017.

[16] James A. Mazer and Jack L. Gallant. Goal-Related Activity in V4 during Free Viewing Visual Search: Evidence for a Ventral Stream Visual Salience Map. *Neuron*, 40(6):1241–1250, December 2003. Publisher: Elsevier.

[17] Jacqueline P. Gottlieb, Makoto Kusunoki, and Michael E. Goldberg. The representation of visual salience in monkey parietal cortex. *Nature*, 391(6666):481–484, January 1998. Number: 6666 Publisher: Nature Publishing Group.

[18] Kirk G. Thompson and Narcisse P. Bichot. A visual salience map in the primate frontal eye field. In *Progress in Brain Research*, volume 147 of *Development, Dynamics and Pathiology of Neuronal Networks: from Molecules to Functional Circuits*, pages 249–262. Elsevier, January 2005.

[19] Richard Veale, Ziad M. Hafed, and Masatoshi Yoshida. How is visual salience computed in the brain? Insights from behaviour, neurobiology and modelling. *Philosophical Transactions of the Royal Society B: Biological Sciences*, 372(1714):20160113, February 2017. Publisher: Royal Society.

[20] Colin Blakemore and Elisabeth A. Tobin. Lateral inhibition between orientation detectors in the cat's visual cortex. *Experimental Brain Research*, 15(4):439–440, September 1972.

[21] Sabine Kastner, Hans-Christoph Nothdurft, and Ivan N. Pigarev. Neuronal responses to orientation and motion contrast in cat striate cortex. *Visual Neuroscience*, 16(3):587–600, May 1999. Publisher: Cambridge University Press.

[22] Hans-Christoph Nothdurft, Jack L. Gallant, and David C. Van Essen. Response modulation by texture surround in primate area V1: Correlates of "popout" under anesthesia. *Visual Neuroscience*, 16(1):15–34, January 1999. Publisher: Cambridge University Press.

[23] H. E. Jones, K. L. Grieve, W. Wang, and A. M. Sillito. Surround Suppression in Primate V1. *Journal of Neurophysiology*, 86(4):2011–2028, October 2001. Publisher: American Physiological Society.

[24] H. E. Jones, W. Wang, and A. M. Sillito. Spatial Organization and Magnitude of Orientation Contrast Interactions in Primate V1. *Journal of Neurophysiology*, 88(5):2796–2808, November 2002. Publisher: American Physiological Society.

[25] Jad Barchini, Xuefeng Shi, Hui Chen, and Jianhua Cang. Bidirectional encoding of motion contrast in the mouse superior colliculus. *eLife*, 7:e35261, July 2018. Publisher: eLife Sciences Publications, Ltd.

[26] Mehran Ahmadlou, Azadeh Tafreshiha, and J. Alexander Heimel. Visual Cortex Limits Pop-Out in the Superior Colliculus of Awake Mice. *Cerebral Cortex*, 27(12):5772–5783, December 2017.

[27] Zhe Li, Ruixiang Wu, and Ya-tang Li. Calcium Imaging in Mouse Superior Colliculus. *JoVE (Journal of Visualized Experiments)*, (194):e65181, April 2023.

[28] Evan H. Feinberg and Markus Meister. Orientation columns in the mouse superior colliculus. *Nature*, 519(7542):229–232, March 2015.

[29] Ya-tang Li, Zeynep Turan, and Markus Meister. Functional architecture of motion direction in the mouse superior colliculus. *Current Biology*, 30(17):3304–3315.e4, September 2020.

[30] Sylvia Schröder, Nicholas A. Steinmetz, Michael Krumin, Marius Pachitariu, Matteo Rizzi, Leon Lagnado, Kenneth D. Harris, and Matteo Carandini. Arousal Modulates Retinal Output. *Neuron*, 107(3):487–495.e9, August 2020.

[31] Yuanming Liu, Elise L. Savier, Victor J. DePiero, Chen Chen, Dana C. Schwalbe, Ruei-Jen Abraham-Fan, Hui Chen, John N. Campbell, and Jianhua Cang. Mapping visual functions onto molecular cell types in the mouse superior colliculus. *Neuron*, 111(12):1876–1886.e5, June 2023.

[32] Lupeng Wang, Rashmi Sarnaik, Krsna Rangarajan, Xiaorong Liu, and Jianhua Cang. Visual receptive field properties of neurons in the superficial superior colliculus of the mouse. *Journal of Neuroscience*, 30(49):16573–16584, December 2010.

[33] Ya-tang Li and Markus Meister. Functional cell types in the mouse superior colliculus. *eLife*, 12:e82367, April 2023. Publisher: eLife Sciences Publications, Ltd.

[34] Samuel D. Gale and Gabe J. Murphy. Distinct representation and distribution of visual information by specific cell types in mouse superficial superior colliculus. *Journal of Neuroscience*, 34(40):13458–13471, October 2014.

[35] Gioia De Franceschi and Samuel G. Solomon. Visual response properties of neurons in the superficial layers of the superior colliculus of awake mouse. *The Journal of Physiology*, 596(24):6307–6332, 2018.

[36] Mehran Ahmadlou and J. Alexander Heimel. Preference for concentric orientations in the mouse superior colliculus. *Nature Communications*, 6(1):6773, April 2015.

[37] Matthew W. Self, Jeannette A. M. Lorteije, Joris Vangeneugden, Enny H. van Beest, Mihaela E. Grigore, Christiaan N. Levelt, J. Alexander Heimel, and Pieter R. Roelfsema. Orientation-Tuned Surround Suppression in Mouse Visual Cortex. *Journal of Neuroscience*, 34(28):9290–9304, July 2014. Publisher: Society for Neuroscience Section: Articles.

[38] D. H. Hubel and T. N. Wiesel. Receptive fields, binocular interaction and functional architecture in the cat's visual cortex. *The Journal of Physiology*, 160(1):106–154.2, January 1962.

[39] D. H. Hubel and T. N. Wiesel. Receptive fields and functional architecture of monkey striate cortex. *The Journal of Physiology*, 195(1):215–243, 1968.

[40] Chih-Yang Chen and Ziad M. Hafed. Orientation and Contrast Tuning Properties and Temporal Flicker Fusion Characteristics of Primate Superior Colliculus Neurons. *Frontiers in Neural Circuits*, 12, 2018.

[41] M. E. Goldberg and R. H. Wurtz. Activity of superior colliculus in behaving monkey. I. Visual receptive fields of single neurons. *Journal of Neurophysiology*, 35(4):542–559, July 1972.

[42] S. V. Girman and R. D. Lund. Most superficial sublamina of rat superior colliculus: neuronal response properties and correlates with perceptual figure-ground segregation. *Journal of Neurophysiology*, 98(1):161–177, July 2007.

[43] B. J. Frost and K. Nakayama. Single visual neurons code opposing motion independent of direction. *Science (New York, N.Y.)*, 220(4598):744–745, May 1983.

[44] Hong-Jin Sun, Jian Zhao, Tracy L. Southall, and Bin Xu. Contextual influences on the directional responses of tectal cells in pigeons. *Visual Neuroscience*, 19(2):133–144, 2002.

[45] Yael Zahar, Hermann Wagner, and Yoram Gutfreund. Responses of Tectal Neurons to Contrasting Stimuli: An Electrophysiological Study in the Barn Owl. *PLOS ONE*, 7(6):e39559, June 2012. Publisher: Public Library of Science.

[46] Yajie Liang, Rongwen Lu, Katharine Borges, and Na Ji. Stimulus edges induce orientation tuning in superior colliculus. *Nature Communications*, 14(1):4756, August 2023. Number: 1 Publisher: Nature Publishing Group.

[47] Xuefeng Shi, Jad Barchini, Hector Acaron Ledesma, David Koren, Yanjiao Jin, Xiaorong Liu, Wei Wei, and Jianhua Cang. Retinal origin of direction selectivity in the superior colliculus. *Nature Neuroscience*, 20(4):550–558, April 2017.

[48] Henry Markram, Maria Toledo-Rodriguez, Yun Wang, Anirudh Gupta, Gilad Silberberg, and Caizhi Wu. Interneurons of the neocortical inhibitory system. *Nature Reviews Neuroscience*, 5(10):793–807, October 2004. Number: 10 Publisher: Nature Publishing Group.

[49] Jose-Manuel Alonso and Luis M. Martinez. Functional connectivity between simple cells and complex cells in cat striate cortex. *Nature Neuroscience*, 1(5):395–403, September 1998. Number: 5 Publisher: Nature Publishing Group.

[50] Ho Ko, Sonja B. Hofer, Bruno Pichler, Katherine A. Buchanan, P. Jesper Sjöström, and Thomas D. Mrsic-Flogel. Functional specificity of local synaptic connections in neocortical networks. *Nature*, 473(7345):87–91, May 2011.

[51] D. Y. Ts'o, C. D. Gilbert, and T. N. Wiesel. Relationships between horizontal interactions and functional architecture in cat striate cortex as revealed by cross-correlation analysis. *Journal of Neuroscience*, 6(4):1160–1170, April 1986. Publisher: Society for Neuroscience Section: Articles.

[52] Sergej Girman and Raymond Lund. Orientation-specific modulation of rat retinal ganglion cell responses and its dependence on relative orientations of the center and surround gratings. *Journal of Neurophysiology*, 104(6):2951–2962, December 2010.

[53] Chuan-Chin Chiao and Richard H. Masland. Contextual tuning of direction-selective retinal ganglion cells. *Nature Neuroscience*, 6(12):1251–1252, December 2003.

[54] Stephen A. Baccus, Bence P. Ölveczky, Mihai Manu, and Markus Meister. A Retinal Circuit That Computes Object Motion. *Journal of Neuroscience*, 28(27):6807–6817, July 2008. Publisher: Society for Neuroscience Section: Articles.

[55] Bence P. Ölveczky, Stephen A. Baccus, and Markus Meister. Segregation of object and background motion in the retina. *Nature*, 423(6938):401–408, May 2003. Number: 6938 Publisher: Nature Publishing Group.

[56] Matthew J. McGinley, Martin Vinck, Jacob Reimer, Renata Batista-Brito, Edward Zagha, Cathryn R. Cadwell, Andreas S. Tolias, Jessica A. Cardin, and David A. McCormick. Waking State: Rapid Variations Modulate Neural and Behavioral Responses. *Neuron*, 87(6):1143–1161, September 2015.

[57] Paul J. May. The mammalian superior colliculus: laminar structure and connections. *Progress in Brain Research*, 151:321–378, January 2006.

[58] Fei Hu and Yang Dan. An inferior-superior colliculus circuit controls auditory cue-directed visual spatial attention. *Neuron*, 110(1):109–119.e3, January 2022.

[59] Ursula C. Dräger and David H. Hubel. Physiology of visual cells in mouse superior colliculus and correlation with somatosensory and auditory input. *Nature*, 253(5488):203, January 1975.

[60] Alexandre Zénon and Richard J. Krauzlis. Attention deficits without cortical neuronal deficits. *Nature*, 489(7416):434–437, September 2012.

[61] Eftychios A. Pnevmatikakis and Andrea Giovannucci. NoRMCorre: An online algorithm for piecewise rigid motion correction of calcium imaging data. *Journal of Neuroscience Methods*, 291:83–94, November 2017.

[62] Werner Göbel and Fritjof Helmchen. In vivo calcium imaging of neural network function. *Physiology*, 22(6):358–365, December 2007.

[63] Aaron M. Kerlin, Mark L. Andermann, Vladimir K. Berezovskii, and R. Clay Reid. Broadly tuned response properties of diverse inhibitory neuron subtypes in mouse visual cortex. *Neuron*, 67(5):858–871, September 2010.

Acknowledgments

Y.-t.L. is supported by the National Natural Science Foundation of China (32271060) and the Beijing Natural Science Foundation (IS23073).

Author contributions

Y.-t.L. supervised the project; Y.-t.L. and R.W. designed the experiments; R.W. collected all the data; Y.-t.L., R.W., J.X., and C.L. analyzed the data; Z.Z. and Y.-t.L. carried out the neural modeling; R.W. and Y.-t.L. prepared figures; Y.-t.L. and L.-y.L. wrote the manuscript.

Competing interests

The authors declare no competing interests.

Data availability

Data will be available in a public repository upon acceptance of the manuscript.

Code availability

Code will be available in a public repository upon acceptance of the manuscript.